Flexural behavior of steel-concrete ultra-shallow floor beams (USFBs) with precast hollow-core slab

Sineval Esteves Pereira Júnior[a], Felipe Piana Vendramell Ferreira[b]*, Konstantinos Daniel Tsavdaridis[c], Silvana De Nardin[b]

[a]Federal University of São Carlos, Department of Civil Engineering, Rod. Washington Luiz, km 235, São Carlos, São Paulo, Brazil.

[b]Federal University of Uberlândia, Faculty of Civil Engineering – Campus Santa Mônica, Uberlândia, Minas Gerais, Brazil

[c]Department of Engineering, School of Science and Technology, City, University of London, Northampton Square, EC1V 0HB, London, UK

**Corresponding author*

Abstract

This paper aims to predict the flexural behavior of steel-concrete composite ultra-shallow floor beams (USFBs) with precast hollow-core slab (PCHCS). A finite element model based on tests is developed. A parametric study is conducted, and the influence of the geometric parameters is discussed. The finite element results were compared with stress block analysis. It was concluded that the modeling with two symmetry planes offered better computational cost, and the flexural behavior of steel concrete USFBs was sensitive to dilation angles. From the parametric study, the models without steel tie bar through the web openings showed lower bearing capacity. The variation of the reinforcement ratio of the concrete topping contributed to the cracking control. The plastic neutral axis position was measured, considering the mid-span vertical displacement at 10 mm, 50 mm and 100 mm. From the stress distribution it was observed that to define the resisting moment, the P.N.A. closest to the top tee can be considered. The theoretical model underestimated the resistance of USFBs with PCHCS.

Keywords: Ultra-shallow floor beams; Steel-concrete composite; Precast hollow-core slab; Finite element method; Design.

E-mail addresses:
fpvferreira@ufu.br (F. P. V. Ferreira)
konstantinos.tsavdaridis@city.ac.uk (K. D. Tsavdaridis)
snardin@ufscar.br (S. De Nardin)

Notation

The following notations and symbols are used in this paper:

A_b	the area of bottom tee
b_f	the flange width
b_{eff}	the effective slab width
b_{min}	the width of the upper flange
c	the depth of concrete topping above the upper flange
D_o	the opening diameter
d_g	the total depth of cellular steel beam
f_{cd}	the design value of concrete compressive strength
f_{ck}	the characteristic compressive cylinder strength of concrete
f_{cm}	the mean value of concrete cylinder compressive strength
f_{ctm}	the mean value of axial tensile strength of concrete
f_y	the yield strength of the steel
f_u	the tensile strength of the steel
L	the span
$M_{pl,Rd}$	the bending resistance of USFB
N_c	the compressive resistance of the concrete slab
N_f	the tensile resistance of the upper flange of cellular steel beam
N_w	the tensile resistance of the upper tee web
n	the number of openings
t_c	the thickness of the concrete topping
t_{fb}	the thickness of the lower flange
t_{ft}	the thickness of the upper flange
t_w	the thickness of the web
y_c	the depth of P.N.A
z_b	the depth of elastic neutral axis
ρ	the reinforcement rate of the concrete topping
φ	the diameter of steel tie bar

1. Introduction

Steel-concrete composite structures are widely used in AEC projects and offer solutions with high structural efficiency and economic viability for both multi-story buildings and bridges. The strength of the materials and the possibility of industrialization of the structural components are factors that favor the use of steel-concrete composite systems, creating solutions for various applications in structural engineering. However, some disadvantages in using the conventional steel-concrete composite beam (i.e., downstand composite beam) have been described by several references, such as: the need for heavier steel profiles with the increase in span, maximizing costs, and the increased of the floor height, mainly for carrying out service installations (hydraulic and electrical) [1–3]. In this scenario, for the replacement of that downstand composite beam, slim-floors[1] beams and ultra-shallow floor beams[2] have been developed.

In Derkowski and Surma [4] was described that the steel-concrete composite slim-floor had its most intense development in the northern European countries, mainly in Sweden. In that scenario, the researchers from the Swedish Institute of Steel Construction, with the aim of reducing the total height of the floor, made a steel profile with an asymmetric section, the lower flange heavier than the upper flange, for placing the concrete slab on top of the lower flange [5]. Lu and Mäkeläinen [6] reported the application of this constructive system in public, commercial and hospital buildings in

[1] Presented by ArcelorMittal
[2] Presented by Kloeckner Metals UK | Westok

Stockholm as a determining factor for the acceptance and use of technology in the following years, contributing significantly to the increase in the number of steel buildings, from 5% of application in projects from commercial buildings in the early 1980s to 50% nationally, and 80% in the Stockholm region by the end of the decade. The growing use in the Nordic countries (Sweden, Finland, Denmark, Norway and Iceland) and the improvement of the slim-floor system led to the spread across the European continent, attracting the interest of researchers and British investors from British Steel [7]. In Ahmed and Tsavdaridis [3] the advances of steel-concrete composite floors were presented considering different types of floor systems. The authors presented different typologies of steel-concrete composite floors, i.e., slim-floor beams and ultra-shallow floor beams (USFBs). The main difference between these steel-concrete composite flooring systems is that the former does not have periodical circular web openings, like the latter. Another important difference concerns the interaction between steel and concrete. In the slim-floor system, the interaction between the concrete slab and the steel profile is made by mechanical devices, such as headed studs shear connectors. As for the USFB, such interaction is made by concrete dowels with steel tie bar through the web openings.

Steel-concrete composite USFBs are systems in which the concrete slab is positioned at the bottom flange of an asymmetric steel cellular profile, and it is made with some connection mechanism responsible for promoting the bond behaviour between the steel and concrete materials. Cellular beams are characterized by the presence of periodical circular web openings created by

the castellation process – a thermal cutting and welding procedures. The increase in flexural stiffness due to expansion of the cross-section height as well as the periodical web openings that favor the integration of services can be highligthed as the key advantages [8–17]. According to Tsavdaridis [18], the use of steel cellular beams can reduce the initial cost of construction by 25% to 30%, reducing the own weight by up to 30% and resulting in savings that can reach 10% of the cost of the structure. Advantages can be highlighted regarding the use of USFBs, such as reducing the floor height (**Fig. 1**), overcoming large spans, reducing local instabilities since the concrete slab restricts displacements along the steel profile, protection against fire and corrosion, fast execution since there is no need for shoring (propping) [19–21]. As the top flange of the steel section acts in conjunction with the concrete slab, the bottom flange is composed of a heavier section, resulting in an increase of the flexural and shear resistances. Generally, the ratio between the bottom and top flange areas varies between 1.5 and 2.5 [22] while UB sections are used for the top tee sections and UC are used for the bottom tee sections.

(a) With profiled steel decking [23]

(b) With precast hollow-core slabs [23]

Fig. 1: Steel-concrete composite USFB

In the last decades, precast concrete hollow-core slabs (PCHCS) have been widely used as an alternative solution to solid and composite slabs with embedded steel formwork [3,24]. The use of PCHCS offers advantages such as the possibility of overcoming large spans, speed, and reduction in construction costs due to their prefabricated nature [25–28]. Pajari and Koukkari [29] described that a structural element, such as the steel profiles that support hollow core slabs, is considered flexible if the shear strength of the slabs is reduced due to deflection. These deflections cause relative slip between the hollow core units and the steel profile. Pajari [30] stated that the connection and friction between the ends of the slab and the beam tend to prevent slippage, resulting in transverse stresses and deformations. According to Hegger et al. [31], it is necessary to decrease the design shear strength of PCHCS on flexible supports. The publication SCI P401 [32] reports that the resistance of PCHCS on flexible supports, which are those (i.e., bottom flange of the steel beam) that undergo deflection, thus increasing the deformations in the PCHCS, can be improved by filling the cores with in-situ concrete, or by placing concrete topping over the PCHCS units. The in-situ concrete topping provides resistance and uniform finishing. Usually, in-

situ concrete topping is 40 to 100 mm of thickness, strength ranges from 25 to 40 MPa, and a small amount of reinforcement to control shrinkage [26,33]. Girhammar and Pajari [34] showed that the concrete topping can be used to improve the shear capacity of hollow core slabs. Derkowski and Surma [4] highlighted that concrete topping not only increased the shear capacity, but also had a positive effect on the stiffness of the steel-concrete composite slim-floor with PCHCS.

In the present study, only the steel-concrete composite USFBs are considered, as shown in **Fig. 1**, as USFB is one of the lease developed and used in practice systems. It is worth noting that studies of composite USFBs began in the 2010s, and the first investigations were carried out at the City, University of London by Tsavdaridis [18] and Huo [35] in collaboration with Westok (Kloeckner Metals, UK). It is important to note that the studies cited here worked only with in-situ concrete. In Tsavdaridis et al. [36] five four-point bending tests were performed. The reference specimen, unlike the others, was not provided with in-situ concrete filling. The authors verified that the concrete filling inhibited the local buckling of the steel cellular profile, thus increasing the resistance. Huo and D'Mello [37,38] assessed the shear transfer mechanisms between steel and concrete by tests. In these studies, the authors predicted the shear resistance of USFB by concrete dowels. The flexural test results showed that the failure mode was a function of the concrete dowel rupture, and the stiffness of the steel-concrete composite USFB in the elastic branch was not influenced by the longitudinal shear resistant mechanism. Braun et al. [39] studied composite USFB with small

openings carrying out tests and finite element analyses. The authors showed that the shear resistance of concrete dowel was efficient, increasing the bearing capacity of this flooring system. In Chen et al. [21], flexural tests were presented. The results indicated that the models with asymmetrical steel profile presented higher bearing capacity and ductility, and the failure was characterized by concrete crushing. Limazie and Chen [40] developed a finite element model to perform a parametric study. In this study, the concrete slab effective width, the concrete topping and the dimensions of the steel cellular profile were investigated. The author concluded that the concrete slab width had no considerable influence on the degree of composite action, the greater the height of the concrete topping, the greater the bearing capacity, and finally as the opening diameter increased, the resistance of USFBs decreased. Subsequently, Limazie and Chen [20] presented an analytical model to predict the shear resistance. It is composed of three portions of resistance: the concrete in compression, the concrete in tension and the steel tie bar through the web opening of the cellular profile. In Ryu et al. [41], the shear transfer mechanism was studied considering the concrete slab composed with biaxial hollow-ball and glass fiber-reinforced plastic plates (GFRP). The authors showed the increase of shear resistance due to the contribution of the GFRPs. At last, in Dai et al. [42], a parametric study employing finite element analyses was presented. The authors verified the increase in the shear resistance in the steel-concrete interface as a function of the increase in the diameter of the concrete dowel. In De O. Ferrante et al. [43] a proposed steel-concrete composite floor system, which was formed by partially-encased

asymmetrical steel profile with periodical rectangular web openings, was investigated by tests. The experimental results agreed with the theorical analyses predicted by the authors. In Alam et al. [44], the behavior of steel-concrete slim-floor systems was investigated in fire situations. According to the authors, the current fire design guidance used for slim-floor beams was highly conservative, in compared with tests results. Kyriakopoulos et al. [45] presented tests and numerical results of the flexural behavior of shallow floor composite beams known as a Deltabeam. In this case, the composite system is formed by steel boxed section with circular web openings. The authors highlighted that ductility depend not only on the steel profile, but also on the ability of the concrete section to resist large strains.

From the current literature, the studies of steel-concrete composite USFBs with PCHCS are scarce. The present paper aims to investigate the flexural behavior of steel-concrete composite USFB with PCHCS. For this, a finite element model is developed based on tests. In the validation study, the influence of the friction coefficient on the steel-concrete interface is analysed. The dilation angle that establishes the constitutive model of concrete is assessed. Two types of symmetry are investigated in order to reduce the computational cost. After the validation step, a parametric study is carried out to verify the influence of the geometric parameters. Finally, the results are discussed considering each parameter evaluated.

2. Finite element model

This section describes the methodology applied to the development of the finite element model via ABAQUS software [46]. Non-linear geometric

194 analysis is considered (*General Static*). The load is applied by automatic
195 increments with a minimum tolerance for convergence of 10^{-5} of the applied
196 external force.

197 2.1. Tests

198 There are no tests of steel-concrete composite USFBs with PCHCS in
199 the literature. Thus the finite element model is developed based on three
200 tests: two of USFBs with in-situ concrete, and another with slim-floor beam
201 with PCHCS. The latter is valid because it is a floor system similar to USFBs.
202 In this context, tests performed by Chen et al. [21], Dai et al. [42] and Souza
203 [47] are considered for the validation study. The geometric characteristics of
204 the tests are shown in **Fig. 2**.

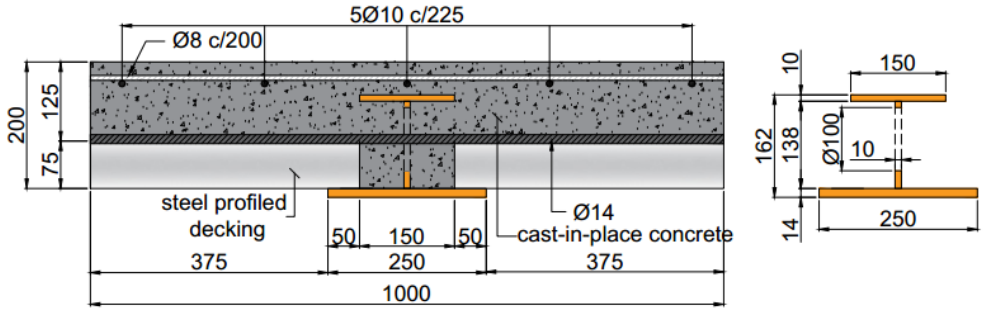

(a) Section [21]

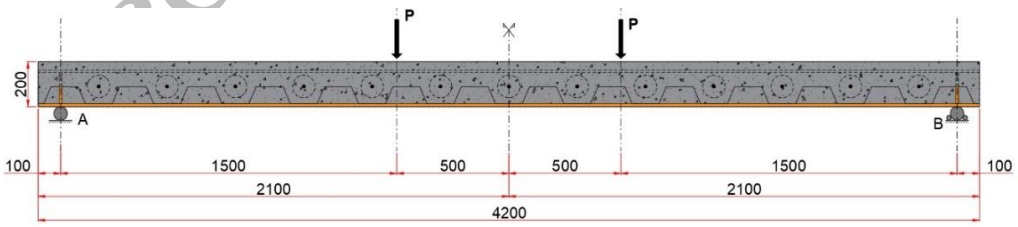

(b) Lateral view [21]

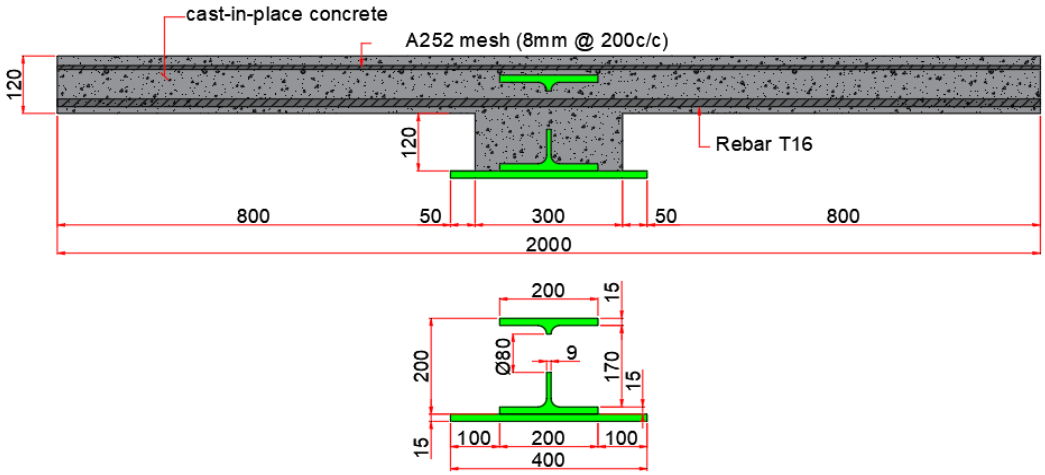

(c) Section [42]

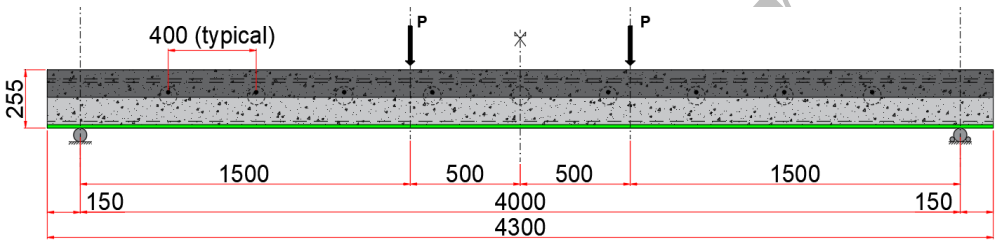

(d) Lateral view [42]

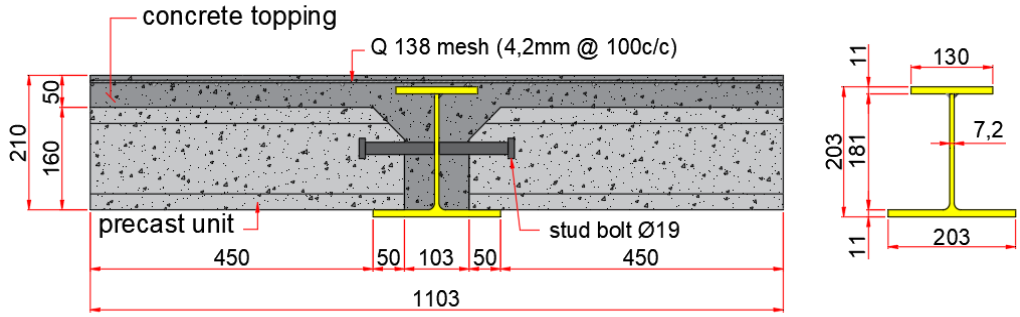

(e) Section [47]

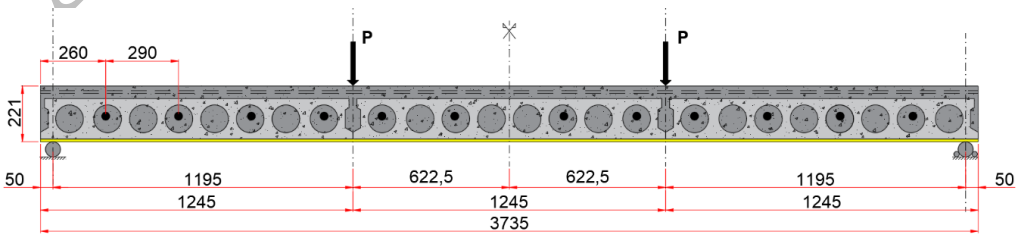

(f) Lateral view [47]

Fig. 2: Geometric characteristics of the tests

2.2. Constitutive models

2.2.1. Concrete

The *Concrete Damage Plasticity* (CDP) [48–50], which allows characterizing the mechanical behavior of concrete both in compression and in tension, is used to simulate the concrete. CDP model can represent the plasticization of concrete from continuous damage assuming that the main failure modes are cracking and crushing. The main parameters needed to define the CDP model are dilation angle (ψ), eccentricity (ϵ), biaxial stress ratio ($\sigma_{b0} / \sigma_{c0}$), shape factor ($K_c$) and viscosity ($\mu$). Except for the dilation angle, the other parameters were considered as standard [46]. There is no consensus among the scientific community regarding the range of values for the dilation angle, as this parameter may represent a condition equivalent to the specific ductility of the concrete structure to be modeled. Rewers [51] concluded that the models became more representative when the dilation angle was greater than 25°. Behnam et al [52] recommended values between 38° and 42°. Nguyen et al [36] verified that the increase in the dilation angle increased the resistance of the PCHCS, indicating satisfactory results for an angle equal to 28º. Qureshi et al. [54], Genikomsou and Polak [55] and Earij et al. [56] used a dilation angle equal to 40º. In a study with steel-concrete composite sections, Katwal et al. [57] obtained satisfactory results for the value of 30º. As shown, the dilation angle must be calibrated as a function of the structural behavior of the element to be represented. In the present study, the dilation angles are defined by means of a sensitivity study.

The stress-strain relationship of concrete under compression described by **Eq. (1)** is built from the formulations and parameters proposed by EC2 [58], where $\eta = \varepsilon_c/\varepsilon_{c1}$ and $k = 1.05 \cdot E_{cm} \cdot |\varepsilon_{c1}|/f_{cm}$. The continuity of the stress-strain beyond the ultimate deformation is established using the equations and parameters of Xu et al. [59] and Pavlovíc et al. [60]. **Eqs. (2-3)** represent the concrete in the descending branch. In these equations the parameters α_a and α_d are defined from the characteristic compressive strength of concrete (f_{ck}).

$$\sigma_c = f_{cm} \cdot \frac{k \cdot \eta - \eta^2}{1 + (k-2) \cdot \eta}, \qquad \eta \leq \varepsilon_{cu1}/\varepsilon_c \tag{1}$$

$$\sigma_c = f_{cm} \cdot [\alpha_a \cdot \eta + (3 - 2\alpha_a) \cdot \eta^2 + (\alpha_a - 2) \cdot \eta^3], \qquad \eta \leq 1 \tag{2}$$

$$\sigma_c = f_{cm} \cdot \frac{\eta}{[\alpha_d \cdot (\eta - 1)^2 + \eta]}, \qquad \eta > 1 \tag{3}$$

For concrete in tension, the stress-strain relationship is calculated from the equations presented in Xu et al. [59], based on GB-50010-2002 [61] (**Eqs. 4-5**), where $\eta = \varepsilon_t/\varepsilon_{tu}$, ε_{tu} is the strain corresponding to the average tensile stress (f_{ctm}).

$$\sigma_t = f_{ctm} \cdot 1{,}2\eta - 0{,}2\eta^6 \,, \eta \leq 1 \tag{4}$$

$$\sigma_t = f_{ctm} \cdot \frac{\eta}{\alpha_t \cdot (\eta - 1)^{1{,}7} + \eta} \,, \eta > 1 \tag{5}$$

The concrete strengths, which are used in numerical modeling, are shown in **Table 1**, according to each reference. The strength values were calculated according to EC2 recommendations.

Table 1: Concrete strength

Reference	In-situ concrete		Precast concrete	
	f_{ck} (MPa)	f_{cm} (MPa)	f_{ck} (MPa)	f_{cm} (MPa)
[21]	29.1	37.1	-	-
[42]	34.5	42.5	-	-
[47]	28.0	36.0	37.0	45.0

2.2.2. Steel

The stress-strain relationship of the embedded steel formwork is assumed to be elastic-perfectly plastic. For the steel mesh, steel tie bar and steel profile, it is used a bilinear model with isotropic hardening. For the cellular profile is adopted the relationships and formulations of the studies by Byfield et al. [62] and Lawson and Saverirajan [9]. The implementation of the stress-strain relationship of steel must be carried out with the real values (**Eqs. 6-7**). The steel strengths are presented in **Table 2-4**.

$$\varepsilon = \ln(\varepsilon_{nom} + 1) \tag{6}$$

$$\sigma = \sigma_{nom} \cdot (1 + \varepsilon_{nom}) \tag{7}$$

Table 2: Steel strengths used in Chen and Limazie model [21]

	f_y (MPa)	f_u (MPa)	E (GPa)
Top flange	462.9	558.8	188
Bottom flange	410.5	553.9	185
Web	462.9	558.7	188
Steel tie bar (14 mm)	548.3	586.7	210
Reinforcement (10 mm)	415.0	588.3	210
Reinforcement (8 mm)	428.3	551.7	210
Steel sheets (1.5 mm)	280	-	210

Table 3: Steel strength used in Dai et al. model [42]

	f_y (MPa)	f_u (MPa)	E (GPa)
HEB200	428	519	210
Bottom plate	455	525	210
Steel tie bar (16 mm)	500[a]	650[a]	210
Steel mesh A252	485[a]	500[a]	210

Table 4: Steel strength used in Souza model [47]

	f_y (MPa)	f_u (MPa)	E (GPa)
W200x46,1	345	450	200
Headed stud (19 mm)	330	430	200
Steel mesh Q138	600	632	210

2.3. Interaction

Although there are numerical studies carried out in USFBs, such as Tsavdaridis et al. [63,64], these studies investigated the shear resistance of partially encased perforated steel beams. Therefore, in this context, the present study considers the investigations carried out as a function of flexural behavior of USFBs, following described. The interaction between the steel profile and the concrete slab is performed using the surface-to-surface contact method, considering normal and tangential behavior. A friction coefficient equal to 0.2 is adopted for the steel-concrete contact [42,65]. Between the contact surfaces of in-situ and prescast concretes, a friction coefficient equal to 1.0 is assigned [66,67]. For the contact between the steel sheets and the cellular beam, a friction coefficient equal to 0.01 is adopted [68]. For the interactions between the concrete and the steel tie bars of the models, tie constraint surfaces is used, which links the nodal elements of two surfaces with different meshes. Embedded region is used between the in-situ concrete topping and the steel mesh.

2.4. Boundary conditions

As a strategy, in a first step, the symmetry modeling method is applied to the three reference models, considering symmetry at XY plane. In the second step, after validation, it is verified the effectiveness of representing only a quarter of the geometry, that is, two planes of symmetry, XY and YZ planes. This leads to a considerable reduction in processing time. **Fig. 3** illustrates the application of boundary conditions.

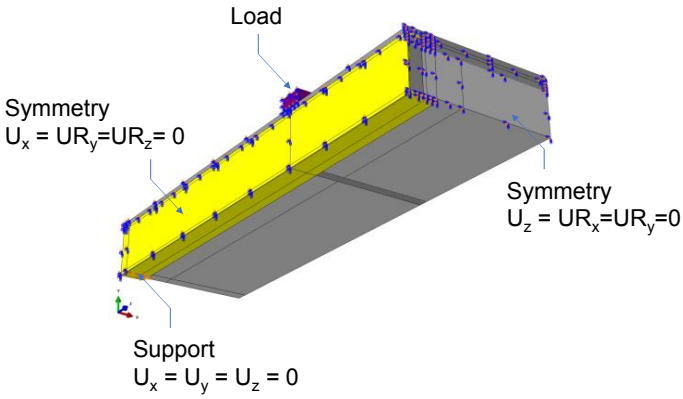

Fig. 3: Boundary conditions of validation study

2.5. Discretization

The finite element discretization for the models by Chen et al. [21], Dai et al. [42] and Souza [47] are presented in **Fig. 4**, **Fig. 5** and **Fig. 6**, respectively. In the modeling of concrete elements, steel profiles, steel tie bar, and shear connectors, C3D8R elements are used. The reinforcements for cracking control are modeled with T3D2 elements. For steel-concretes composite slab, embedded steel formwork is discretized with S4R elements.

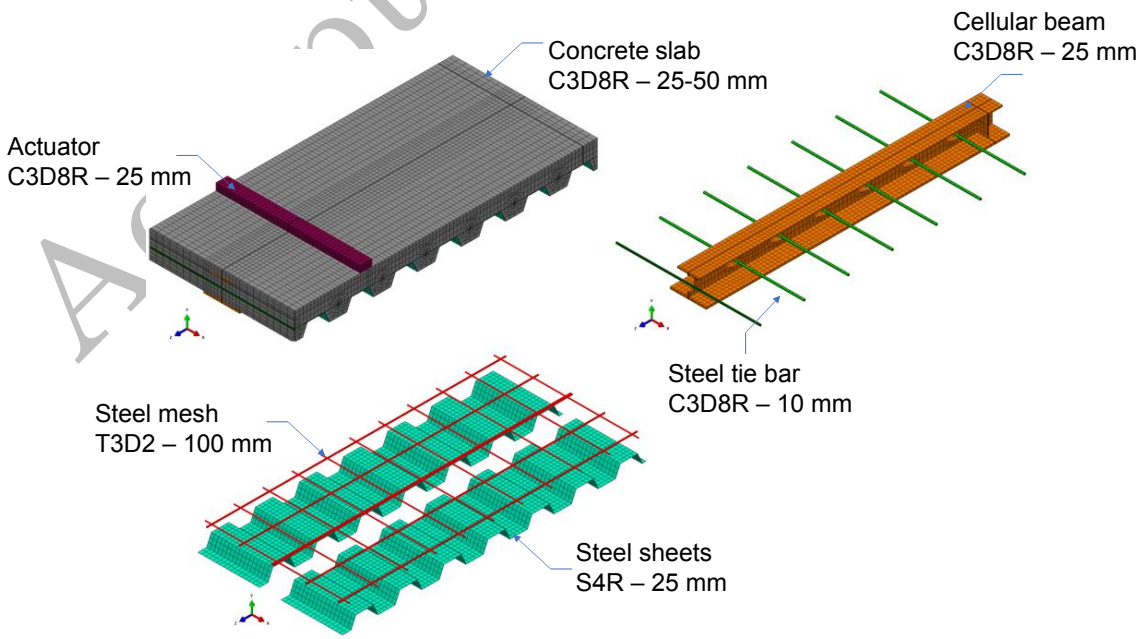

Fig. 4: Discretization for the Chen et al. [21] model

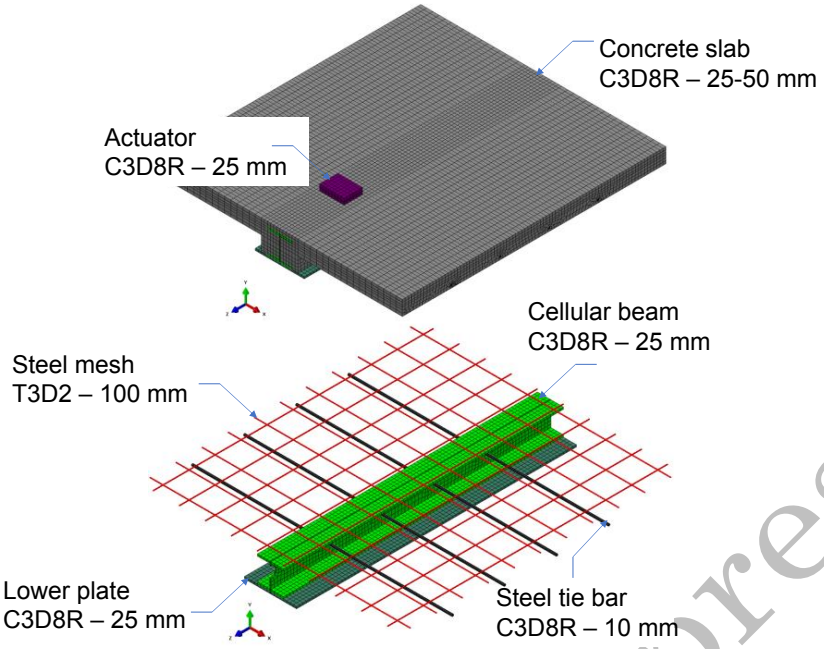

Fig. 5: Discretization for the Dai et al. [42] model

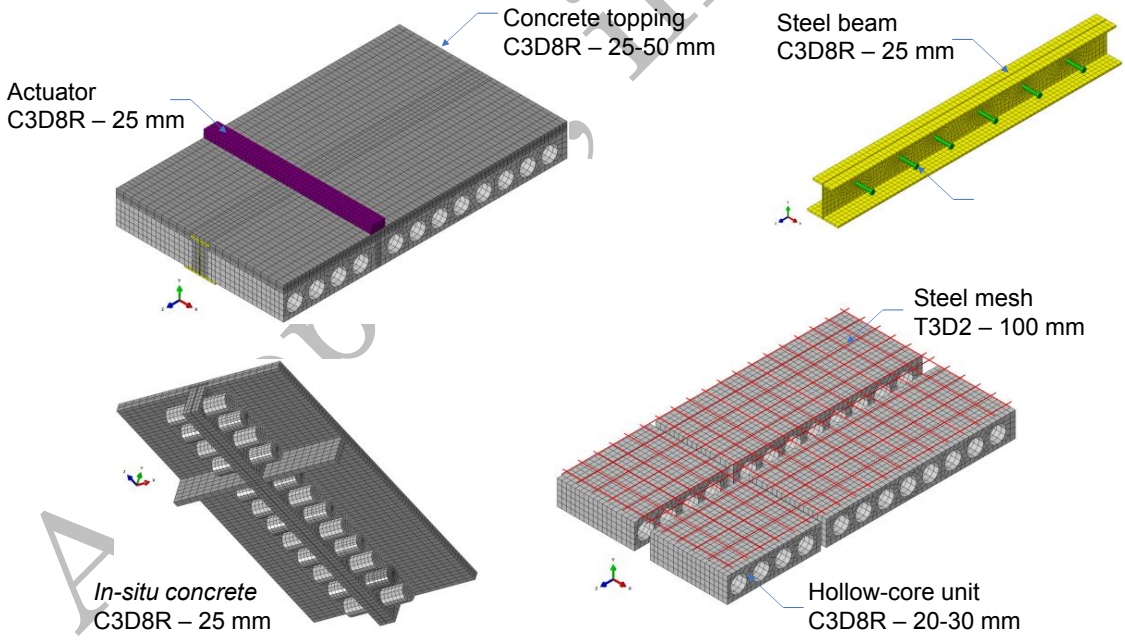

Fig. 6: Discretization for the Souza [47] model

2.6. Validation results

2.6.1. Symmetry

As previously described in section 2.4, a study was carried out to reduce the computational cost, considering one and two planes of symmetry. Next in

Fig. 7, the response is illustrated by load-displacement relationships, considering as an example the test carried out by Souza [47]. For the same processor, modeling with only one symmetry plane took approximately 7 hours to complete, while modeling with two symmetry planes took 3 hours. Thus, as there was no difference in the response between the analyses, the modeling with two symmetry planes offers better computational cost.

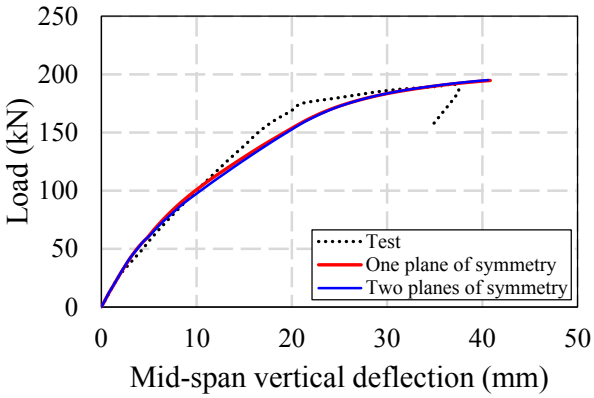

Fig. 7: Influence of symmetry on boundary conditions

2.6.2. Dilation Angle

Fig. 8 shows the influence of the dilation angle. In general, the greater the dilation angle, the greater the resistance of the structural system. However, it is noted that for the model by Chen et al. [21] (**Fig. 8a**), the value of 40º was closer to the test result, while the 30º and 20º values were closer to the models by Dai et al. [42] (**Fig. 8b**) and Souza [47] (**Fig. 8c**), respectively. This last model is modelled with PCHCS. It is important to highlight that in the study carried out by Nguyen et al. [53], the value of 28º was recommended for PCHCS.

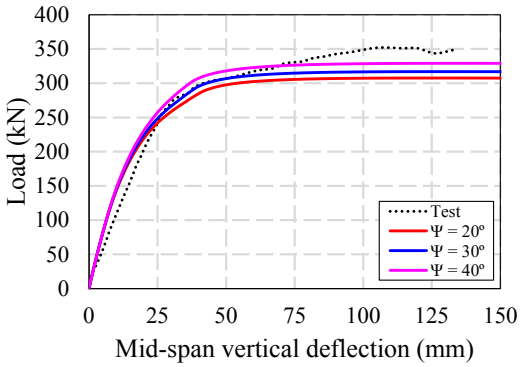

(a) Model of Chen et al. [21]

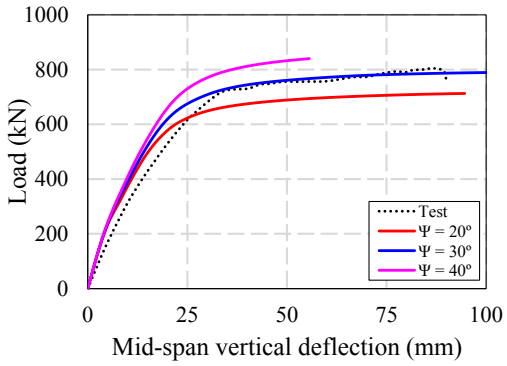

(b) Model of Dai et al. [42]

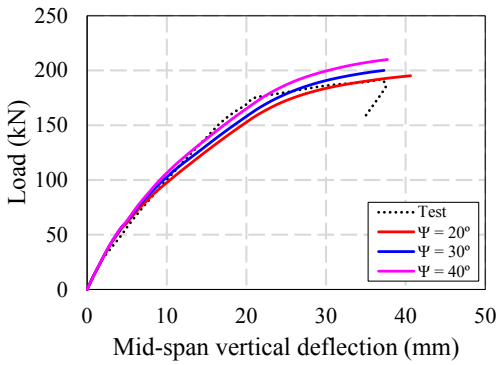

(c) Model of Souza [47]

Fig. 8: Influence of dilation angle

2.6.3. Elaborated models

Fig. 9 shows the results by force-displacment relationship. Chen et al. [21] identified crushing of the concrete in the compressed region of uniform bending as failure mode (**Fig. 10a**). The numerical model identified a failure mode similar to that described by the authors, as shown in **Fig. 10b**. In relation to the test performed by Dai et al. [42], few details about the failure modes were presented. However, the authors described the occurrence of cracking regions. The numerical model showed the cracking regions (**Fig. 10c**), and it was also possible to verify that the steel section presented yield

328 regions, as shown in **Fig. 10d**. Finally, during the Souza [47] test longitudinal
329 cracking was identified in the concrete topping (**Fig. 10e**), and yielding of the
330 steel profile (**Fig. 10f**). **Table 5** summarizes the results.

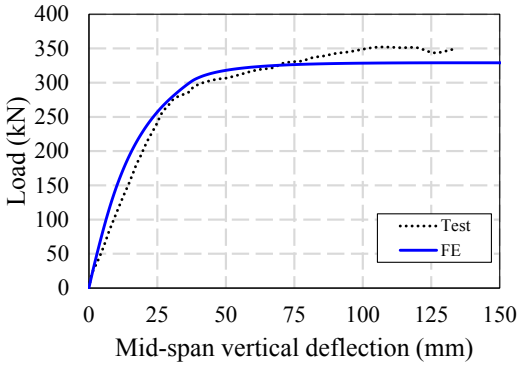

(a) Model of Chen et al. [21]

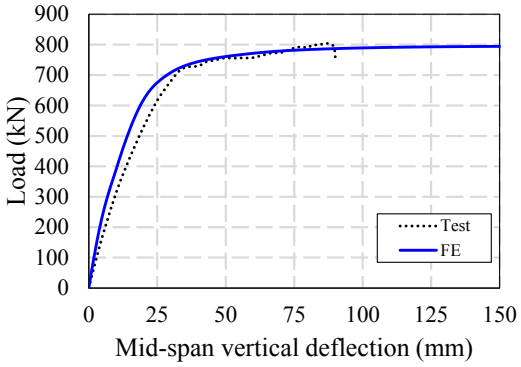

(b) Model of Dai et al. [42]

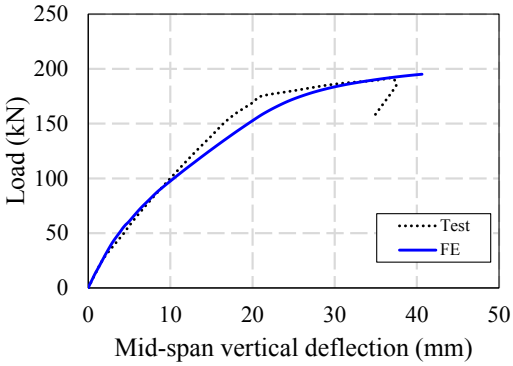

(c) Model of Souza [47]

331 Fig. 9: Final results

(a) Test [21]

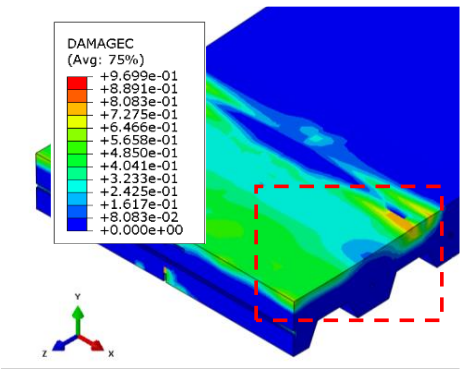

(b) Numerical model

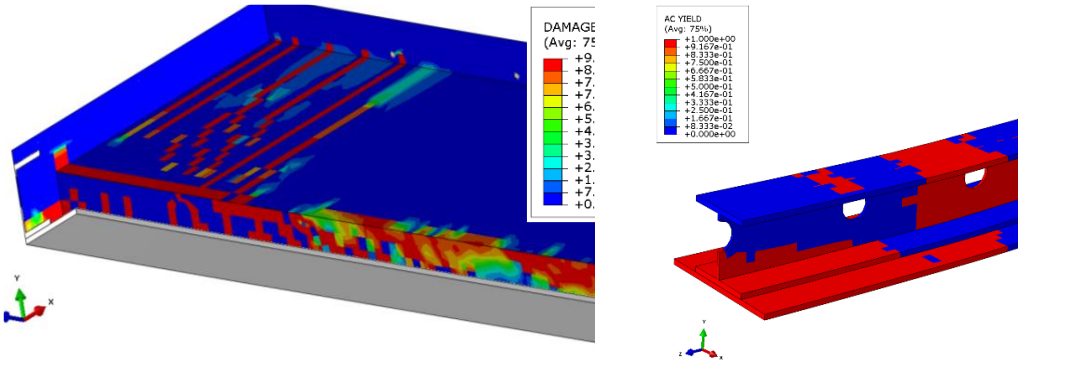

(c) Damage in slab (d) Steel yielding

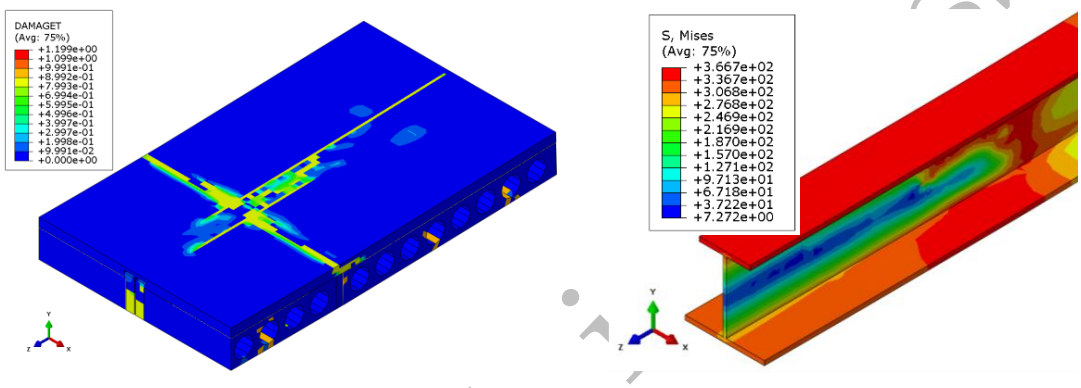

(a) Longitudinal crack in concrete topping (b) Steel yielding

Fig. 10: Final configurations of finite element models

Table 5: Final results

Model	Reference	F_{test} (kN)	F_{FE} (kN)	F_{test}/F_{FE}
1	Chen et al. [21]	349	329	1.06
2	Dai et al. [42]	758	787	0.96
3	Souza [47]	194.1	192.0	1.01
			Var.	0.2%
			S.D.	4.1%

3. Parametric study

With the results presented in the validation study, it is possible to state that the finite element model was validated. As the steel-concrete composite cellular slim floor with PCHCS are structures similar to those used in the validation study, it is possible to develop a numerical model capable of

predicting the flexural behavior, and consequently, carry out a study to verify the influence of geometrical parameters. This will be done using the same boundary conditions applied previously, as shown in **Fig. 11**.

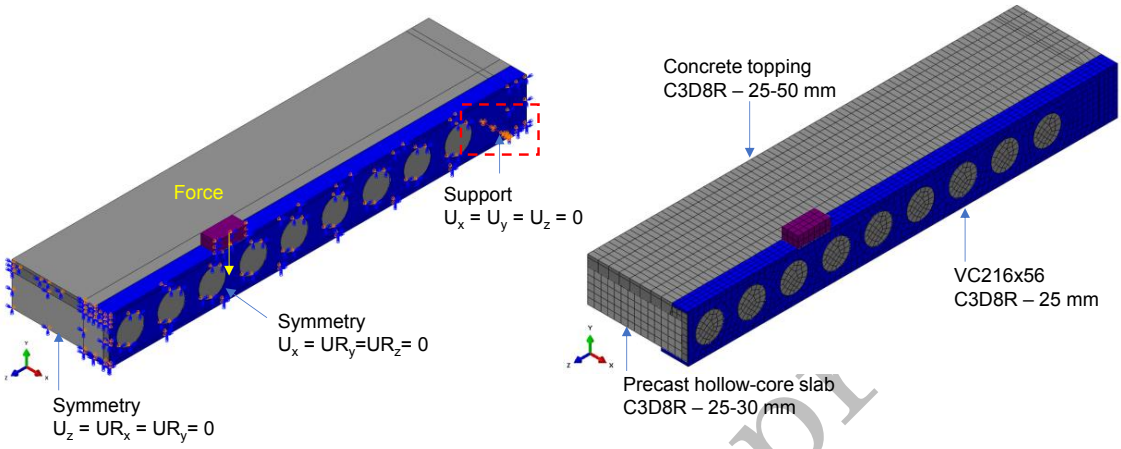

Fig. 11: Finite element model of steel-concrete composite cellular slim floor beams with PCHCS

For the parametric study, a reference model was developed. This reference model will be used to compare the other models, considering the variation of parameters, such as: diameter of steel tie bar (φ) considering the number of bars between the mid-span and supports, thickness of the concrete topping (t_c), the reinforcement rate of the concrete topping (ρ), the opening diameter (D_o), thickness of the lower flange (t_{fb}), thickness of the web (t_w), thickness of the upper flange (t_{ft}) and the number of openings (n). The steel yield (f_y) and in-situ concrete (f_{ck}) strengths remained constant, equal to 250 MPa and 30 MPa, respectively. **Fig. 12** and **Table 6** present the parameters and models of the parametric study, and the geometric characteristics of the parametric study are presented in **Fig. 13**.

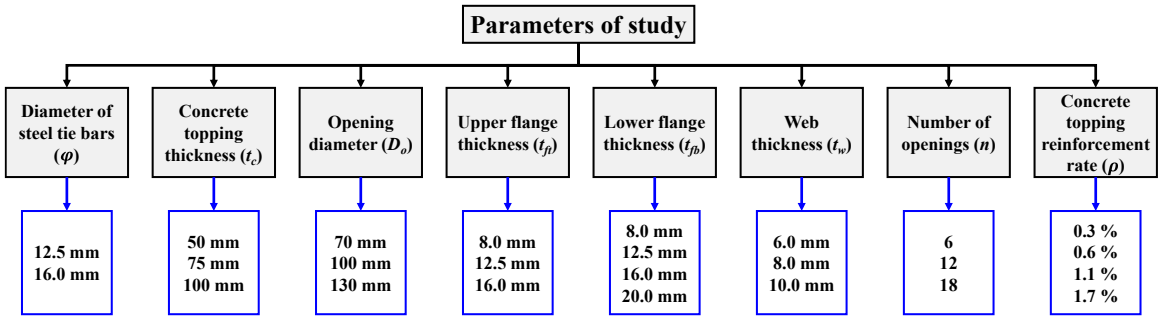

Fig. 12: Parameters of study

Table 6: Parametric study

Model	φ (mm)	t_c (mm)	D_o (mm)	t_{fb} (mm)	t_w (mm)	t_{ft} (mm)	n	ρ (%)
Reference	-	50	130	16	8	12.5	18	0.6
1	2x12.5	50	130	16	8	12.5	18	0.6
2	2x16.0	50	130	16	8	12.5	18	0.6
3	3x12.5	50	130	16	8	12.5	18	0.6
4	3x16.0	50	130	16	8	12.5	18	0.6
5	4x12.5	50	130	16	8	12.5	18	0.6
6	4x16.0	50	130	16	8	12.5	18	0.6
7	-	50+25	130	16	8	12.5	18	0.6
8	-	50+50	130	16	8	12.5	18	0.6
9	-	50	70	16	8	12.5	18	0.6
10	-	50	100	16	8	12.5	18	0.6
11	-	50	145	16	8	12.5	18	0.6
12	-	50	160	16	8	12.5	18	0.6
13	-	50	130	8.0	8	12.5	18	0.6
14	-	50	130	12.5	8	12.5	18	0.6
15	-	50	130	20.0	8	12.5	18	0.6
16	-	50	130	16	6	12.5	18	0.6
17	-	50	130	16	10	12.5	18	0.6
18	-	50	130	16	8	8.0	18	0.6
19	-	50	130	16	8	16.0	18	0.6
20	-	50	130	16	8	12.5	12	0.6
21	3x12.5	50	130	16	8	12.5	12	0.6
22	3x16.0	50	130	16	8	12.5	12	0.6
23	-	50	130	16	8	12.5	6	0.6
24	3x12.5	50	130	16	8	12.5	6	0.6
25	3x16.0	50	130	16	8	12.5	6	0.6
26	-	50	130	16	8	12.5	18	0.3
27	-	50	130	16	8	12.5	18	1.1
28	-	50	130	16	8	12.5	18	1.7

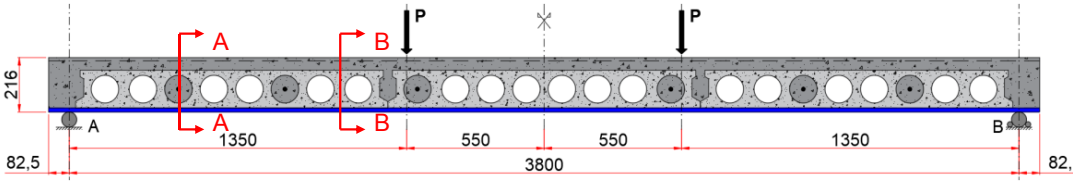

(a) Lateral view

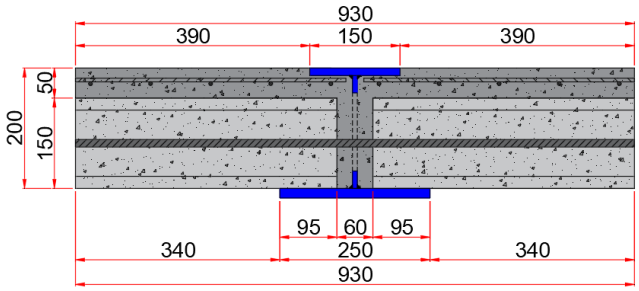

(b) Section A-A

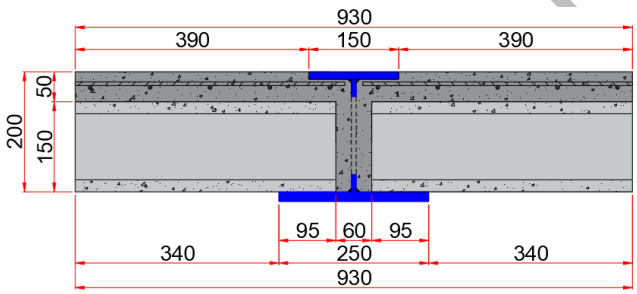

(c) Section B-B

Fig. 13: Geometry scheme for parametric study

4. Results and discussion

4.1. Steel tie bar

The reference model does not present steel tie bar through the openings. Although the reference model showed the lowest resistance and stiffness, all models showed a linear behavior up to a force of 125 kN. From this stage, a non-linearity of the curve began, which indicated the principle of yielding of the materials. **Fig. 14** illustrates the results, considering the two (**Fig. 14a**), three (**Fig. 14b**) and four (**Fig. 14c**) reinforcements, respectively.

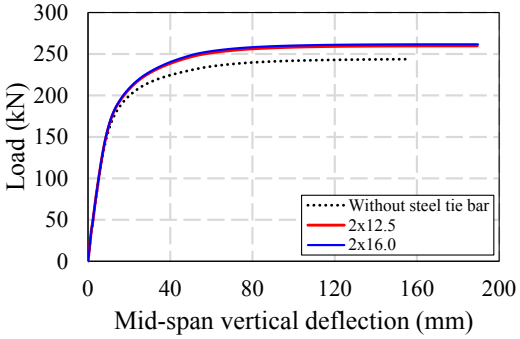

(a) Two steel tie bar

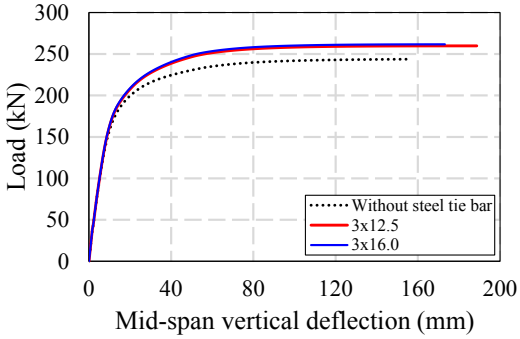

(b) Three steel tie bar

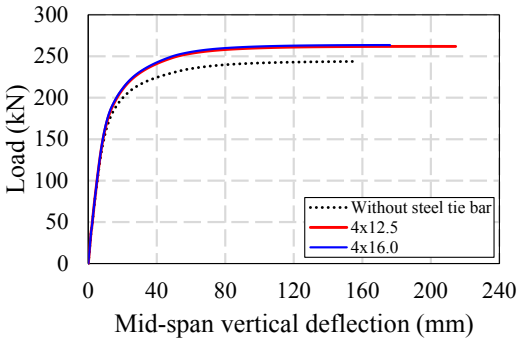

(c) Four steel tie bar

Fig. 14: Influence of the steel tie bar

The presence of the steel tie bar favored the increase of the resistance in relation to the model without the bar. It was observed that the 2x12.5 and 2x16.0 models showed an increase in the bending resistance of 6.7% and 7.5%, respectively, in relation to the reference model, without the steel tie bar. Regarding the models with three bars, an increase of 6.8% and 7.6% was verified for the 3x12.5 and 3x16.0 models, respectively, in comparison with the reference model. Finally, for the models with four bars, an increase in the bending resistance of 7.5% and 8.2% was verified, considering the 3x12.5 and 3x16.0 models, respectively, in relation to the reference model. As a reference,

the amount of 2 bars with a diameter of 12.5 mm indicated the minimum limit for application in this type of composite section.

Fig. 15a shows the distribution of von Mises stresses in the steel tie bars of the 3x12.5 model, where it is possible to see the beginning of plasticization of the bar close to the support. The stress distribution in the axial direction of the 3x16.0 model bars (**Fig. 15b**) indicated significant tensile stresses in the first two bars, with low stress on the third bar.

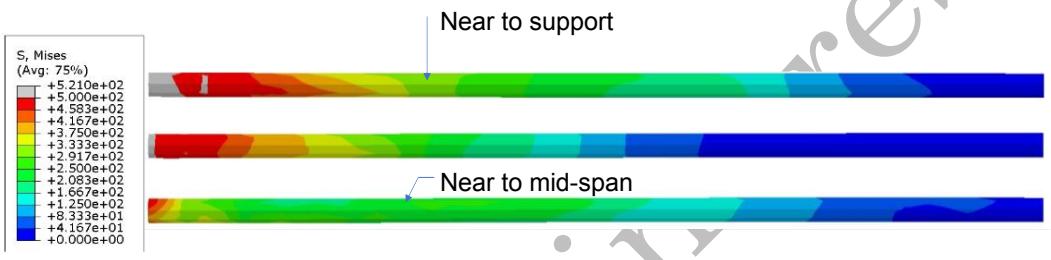

(a) Model 3x12.5

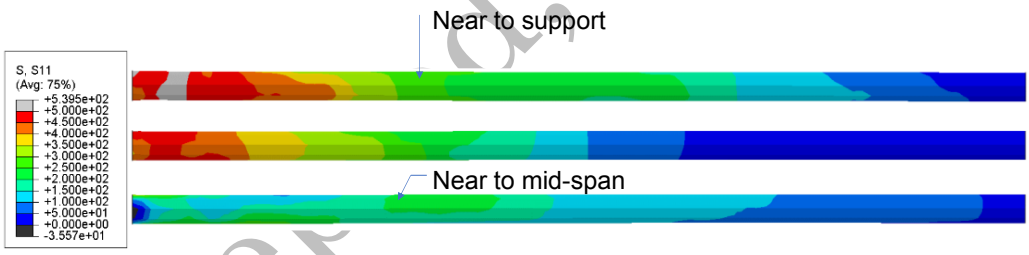

(b) Model 3x16.0

Fig. 15: Steel tie bar; von Mises stresses (in MPa)

4.2. Concrete topping thickness

The concrete topping thickness of the reference model is 50 mm. Increasing the thickness considerably increases the resistance and stiffness of the composite section, as illustrated in **Fig. 16**. The models with concrete topping thickness equal to 75 mm and 100 mm showed an increase in bending resistance equal to 15.7% and 30.52%, respectively, in compared to the

392 reference model. For the models of with 75 mm and 100 mm of thicknesses,
393 the numerical analysis showed a significant reduction of plastic deformations
394 in the compressed region and in the area of application of the force.

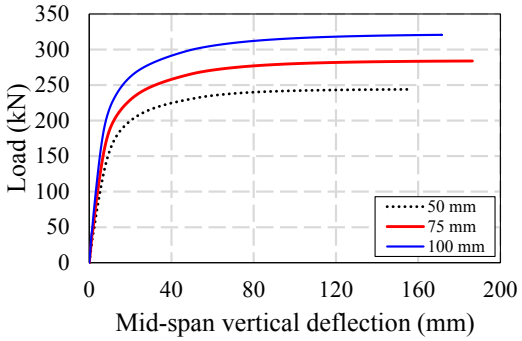

395

396 Fig. 16: Influence of concrete topping thickness

397 Although with the variation reinforcement rate of concrete topping
398 there was no significant increase in the bending resistance (less than 1%), the
399 variation of the reinforcement ratio for cracking control indicated a relevant
400 contribution to the compressed region and in the region of force application,
401 as shown in **Fig. 17**. Therefore, the higher the reinforcement ratio, the smaller
402 the cracked region in the concrete topping.

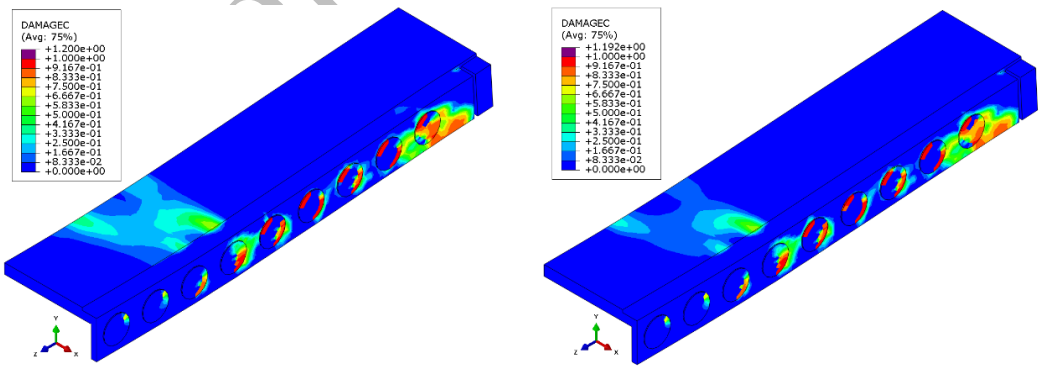

(a) ρ =0.3% (b) ρ =0.6% (Reference model)

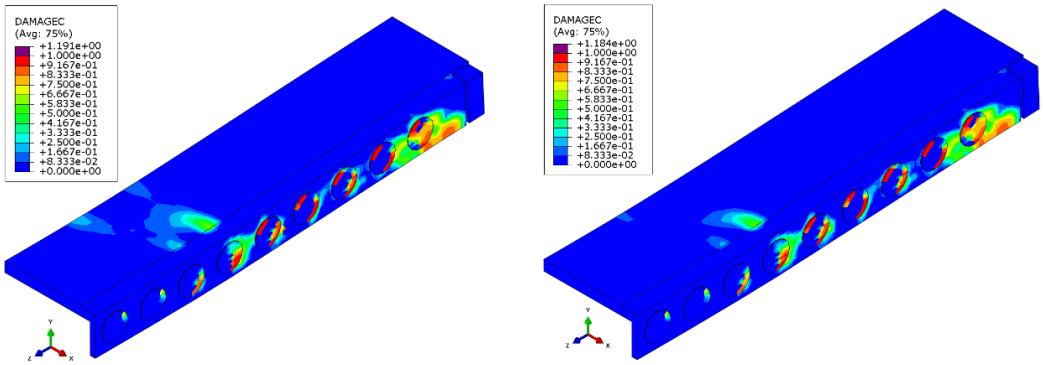

(c) ρ =1.1% (d) ρ =1.7%

Fig. 17: Influence of reinforcement rate of concrete topping

4.3. Diameter opening

The reference model has an opening diameter of 130 mm. **Fig. 18** illustrates the results regarding the opening diameter variation. The results showed that the smaller the diameter, the greater the resistance of the structural system. The model with a diameter of 70 mm had an increase in the bending resistance of 9.5% in compared to the reference model. Regarding the 130 mm and 145 mm models, there were no significant differences in compared to the reference model. On the other hand, for the 160 mm diameter model, a reduction of 32% in the bending resistance was verified. **Fig. 19** shows the von Mises stress distribution. It was verified the appearance of plastic hinges in the web-post. This condition may result from the concrete crushing in the compressed region with excessive deformation.

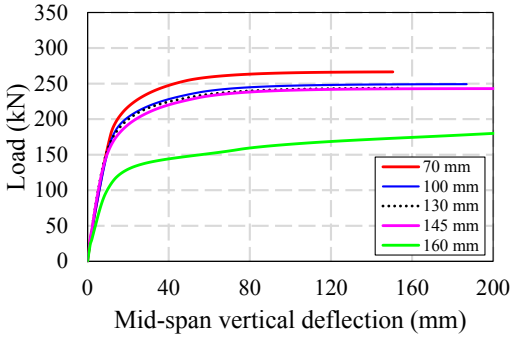

Fig. 18: Influence of diameter opening

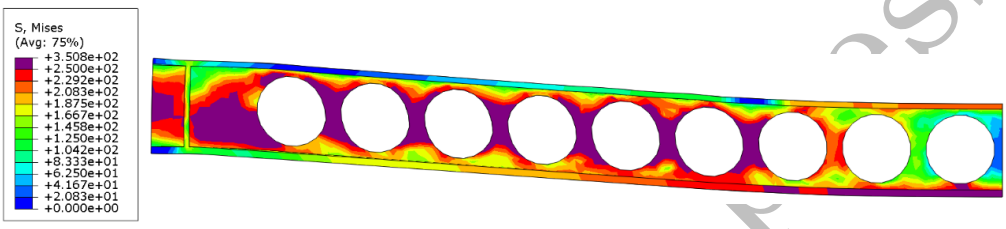

Fig. 19: Model with 160 mm of opening diameter; von Mises stresses (MPa)

4.4. Flanges and web thicknesses

The reference model has a lower flange thickness, and it is equal to 16 mm. **Fig 20a** illustrates the flexural behavior, regarding the variations of thicknesses. The reduction in the thickness of the lower flange indicated a drop in resisntance and loss of stiffness. For the models with 8 mm and 12.5 mm, a reduction of 10.4% and 4.4% in the bending resistance, respectively, was verified, in comparison to the reference model. On the other hand, for the 20 mm model compared to the reference model, a 3.6% of increase in the bending resistance was observed. The variation in the thickness of the upper flange (**Fig. 20b**) did not present a significant influence (less than 2.2%), due to the strong contribution of the concrete slab to the compressive strength. Finally, **Fig. 20c** highlight the variation of the web thickness. This parameter showed great influence, with significant variation in resistance and stiffness.

The reference model has a web thickness of 8 mm. The 6 mm thick model showed a drop of 22% in the bending resistance compared to the reference model, whose web thickness is 2 mm greater. The reduction of the slope of the tangent line to the linear branch of the model evidences the decrease in stiffness. The 10 mm thick model, on the other hand, presented an increase of 9% in compared to the reference model. The results corroborate the critical analysis of the parameters related to the web of the cellular profile, indicating susceptibility to the formation of plastic hinges in the web-post, as one of the collapse modes.

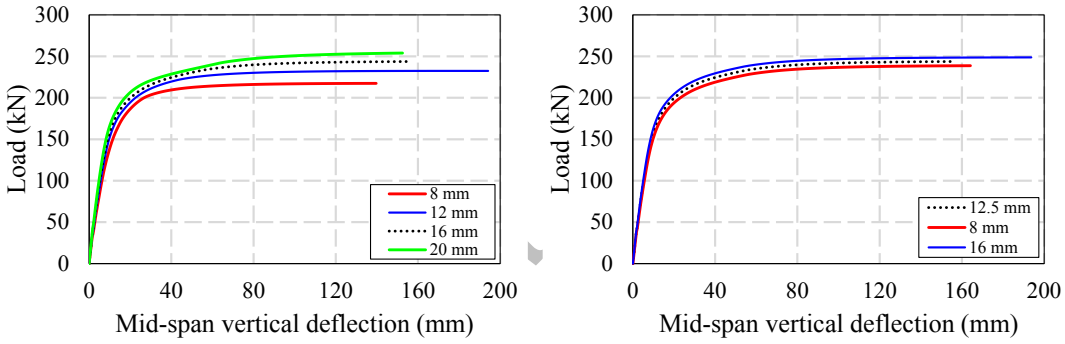

(a) Influence of bottom flange thickness

(b) Influence of top flange thickness

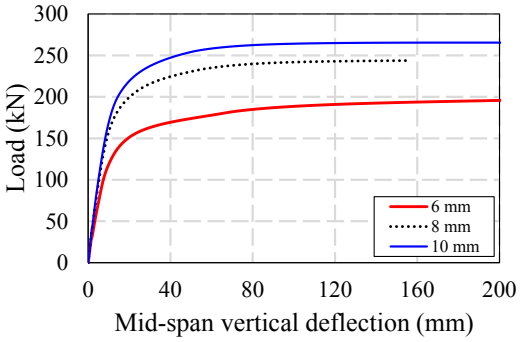

(c) Influence of web thickness

Fig. 20: Influence of thicknesses

443 4.5. Number of openings

444 The purpose of varying the number of openings was to investigate the
445 variation in resistance as a function of the number of concrete dowels. The
446 reference model has 18 openings. The reference model, without steel tie bar
447 through the openings, presented the lowest values of applied force, with
448 greater vertical displacement at mid-span (**Fig 21a**). In addition, the model
449 with twelve openings, without crossbars, showed an increase of 7.7% in the
450 bending resistance in compared to the reference model, indicating that the
451 reduction of shear connectors as a concrete dowel effect was not decisive for
452 the performance of the model, although it showed lower ductility. For the
453 model without steel tie bar and six openings, the increase was 13.4%, in
454 compared to the reference model. The model with 12.5 mm bars (**Fig. 21b**)
455 showed a slight reduction in applied force. The model with six openings and
456 6 crossbars of 16 mm passing through the six openings presented greater
457 resistance and greater stiffness (**Fig. 21c**). In this context, the bending
458 resistance increase was 5.4% and 12.7%, considering the models with twelve
459 and six openings, respectively, in comparison to the reference model. It is
460 possible to state the significant contribution of the steel tie bar, mainly for
461 the reduced number of openings, as analysed. For the models with 16.0 mm
462 bars, the resistance increase was similar to 12.5mm bar models.

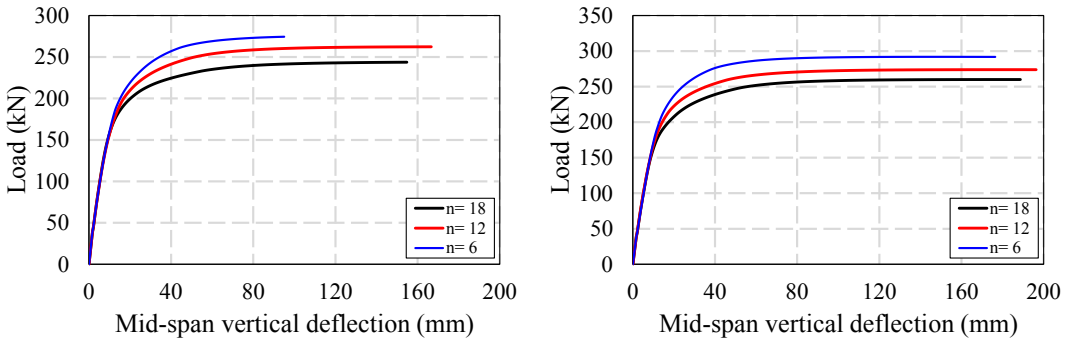

(a) Without steel tie bar (b) Steel bars 3x12.5

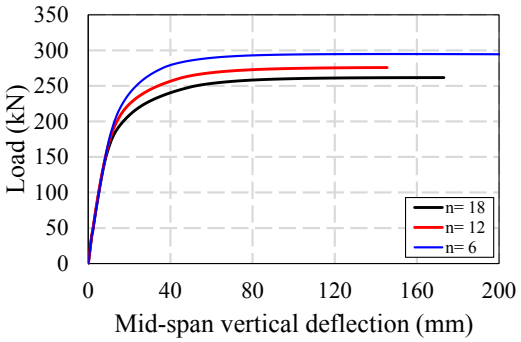

(c) Steel bars 3x16.0

Fig. 21: Influence of the number of openings

Fig. 22 shows the stress distribution in the cellular profile of the model with six openings, but without steel tie bars, for the maximum applied force. The stresses in the cellular profile indicate the yielding of the lower tee section and the cracking of the concrete, configuring a change in the mode of failure in relation to the reference model.

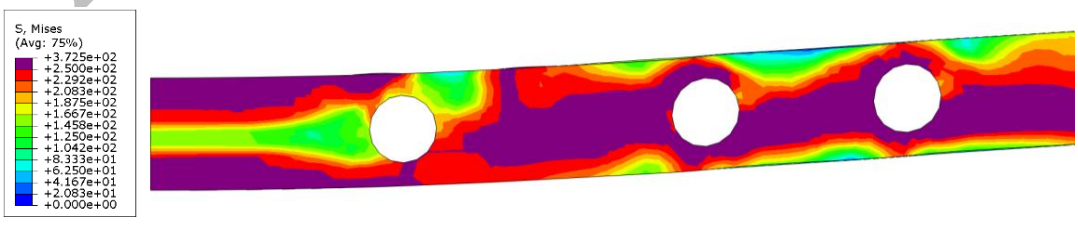

(a) von Mises stress in steel cellular beam (in MPa)

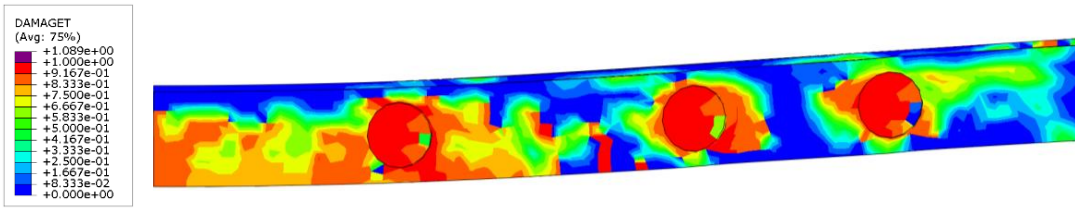

(b) Concrete tensile damage

Fig. 22: Model with six web openings and without steel tie bar

4.6. Position of plastic neutral axis (P.N.A)

Fig. 23 shows some examples of the variation of the P.N.A position measured in three stages throughout the processing, considering the mid-span vertical displacement at 10 mm, 50 mm and 100 mm. The stress values were calculated by linear interpolation of the nodes between the top of the steel profile and the bottom face of the bottom flange, considering a discretization of 1,000 points. This discretization is done automatically by the Abaqus software, through the stress linearization tool.

The results showed that, in the initial phase of loading, the P.N.A was positioned at the opening of the cellular steel profile. With the beginning of plasticization, there is a deviance in the stress distribution, possibly associated with the localized effect of low stresses in the web-post region at mid-span, which tends to oscillate between tensile and compressive stresses. This effect generates a stress drop at web-post, characterizing an area of low tensile stresses, which particularizes the analysis of the P.N.A position. The simulations indicated that this is a localized effect in the constant bending moment region. The transition between the compressive and tensile stresses occurred close to the top tee, still in the region of the opening of the steel cellular profile. This characterization of the stress distribution showed that,

489 for analysis and determination of the resisting moment, the P.N.A closest to
490 the top tee can be considered in the analysis.

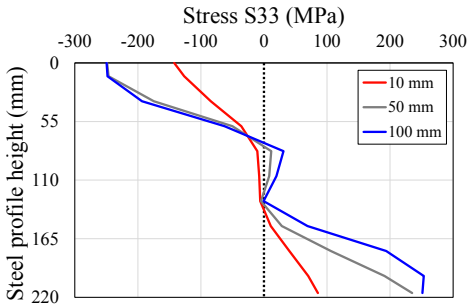

(a) Reference model

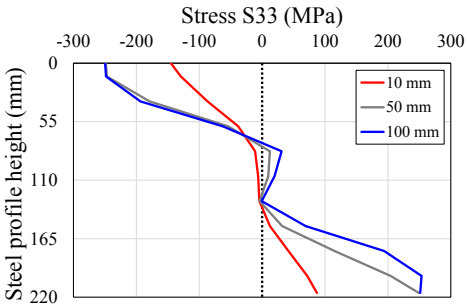

(b) Model 3

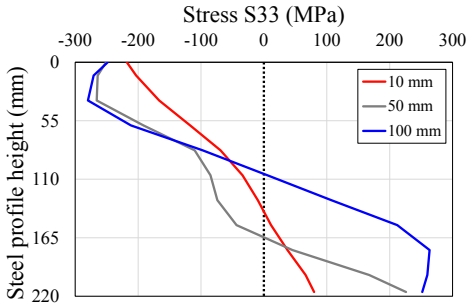

(c) Model 9

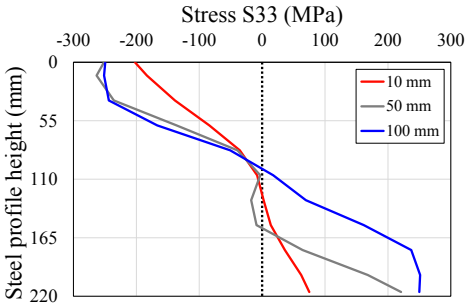

(d) Model 10

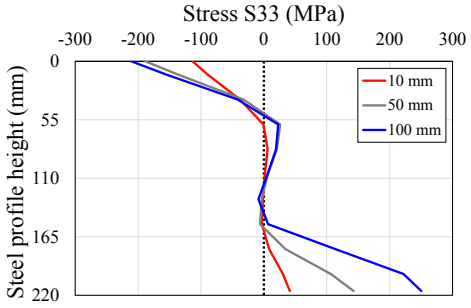

(e) Model 12

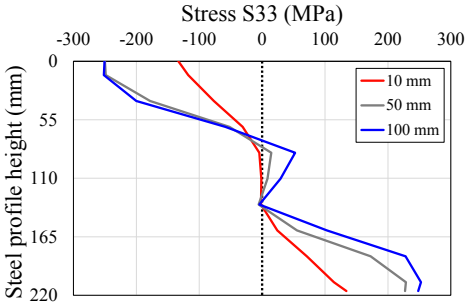

(f) Model 13

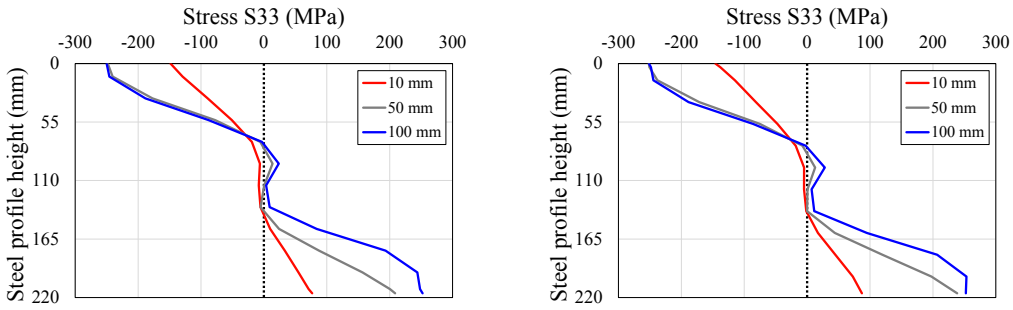

(g) Model 15 (h) Model 19

Fig. 23: Plastic neutral axis position

5. Design of steel-concrete composite ultra-shallow floor beams with precast hollow-core slab

In this section, the stress block analysis is compared with the finite element results, considering full interaction, according to the stress profiles presented previously. The position of the plastic neutral axis (P.N.A) is estimated according to the theoretical models. The calculation model that is presented here is based on the works of Tsavdaridis [18] and Huo [35]. It is important to highlight that the experimental and computational works of these references were employed for the production of the Steel Construction Institute (SCI) publication titled "Design of composite beams with large web openings" [69].

Thus, the plastic bending resistance of composite USFBs is presented, considering PCHCS. In this context, considering full interaction, the P.N.A lies on concrete topping passing through the flange (**Fig. 24a**) or web (**Fig. 24b**) of the top tee, since the axial resistance of the bottom tee (N_b) is less than the sum of the axial resistances of the top tee (N_t) and the concrete topping (N_c). It is important to highlight that the analysis is made in critical section,

509 that is, the one in the region of constant bending moment that was not filled
510 with concrete.

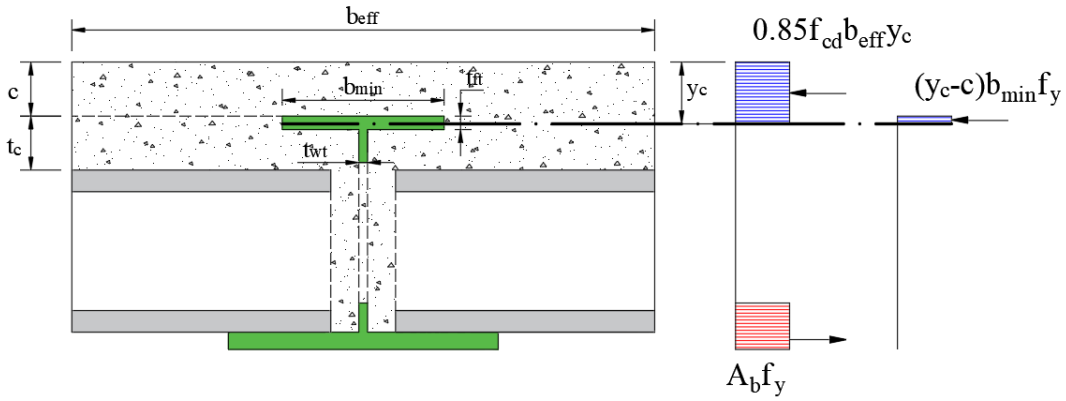

(a) P.N.A lies on flange

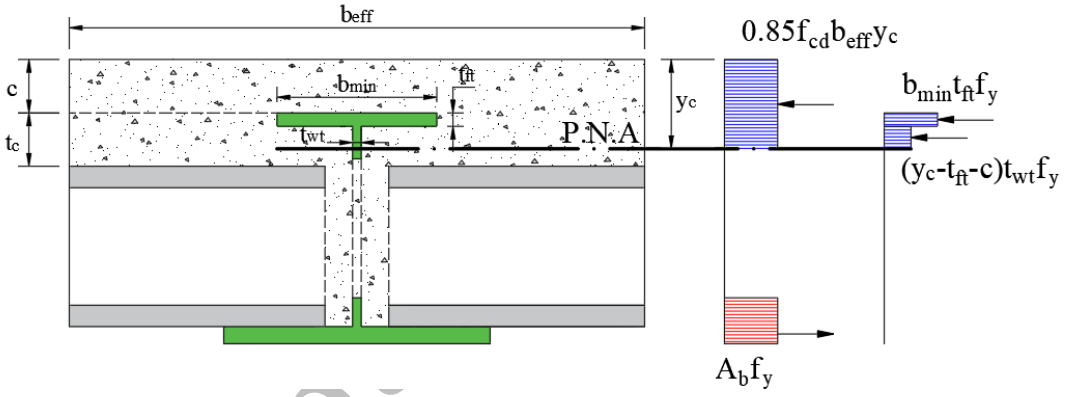

(b) P.N.A lies on web

511 Fig. 24: P.N.A lies on top tee

512 In this scenario, the bending resistance of steel-concrete composite USFBs
513 can be calculated, according to **Eqs. (8)-(18)** that are presented below:

514 • <u>P.N.A lies on flange</u>:

$$b_{eff} = L/4 \tag{8}$$

$$f_{cd} = f_{ck}/1.5 \tag{9}$$

$$y_c = \frac{(A_b + b_{min}c)f_y}{0.85f_{cd}b_{eff} + b_{min}f_y} \tag{10}$$

$$N_f = b_{min}(y_c - c)f_y \tag{11}$$

$$N_c = 0.85 f_{cd} b_{eff} y_c \tag{12}$$

$$M_{pl,Rd} = N_f\left[d_g - z_b - 0.5(y_c - c)\right] + N_c\left(d_g + c - z_b - 0.5y_c\right) \tag{13}$$

- P.N.A lies on web:

$$y_c = \frac{\left(A_b - b_{min}t_{ft} + ct_{wt} + t_{ft}t_{wt}\right)f_y}{0.85 f_{cd} b_{eff} + t_{wt}f_y} \tag{14}$$

$$N_f = b_{min} t_{ft} f_y \tag{15}$$

$$N_w = \left(y_c - t_{ft} - c\right)t_{wt} f_y \tag{16}$$

$$N_c = 0.85 f_{cd} b_{eff} y_c \tag{17}$$

$$M_{pl,Rd} = N_f\left(d_g - z_b - 0.5t_{ft}\right) + N_w\left[d_g - z_b - t_{ft} - 0.5\left(y_c - c - t_{ft}\right)\right] + N_c\left(d_g - z_b - 0.5y_c\right) \tag{18}$$

Fig. 25 presents the numerical results in comparison with the theoretical model. As illustrated, the mean, standard deviation and variance of the $M_{FE}/M_{pl,Rd}$ ratio were equal to 1.40, 12.80% and 1.64%. This means that the theoretical model underestimates the resistance of USFBs with PCHCS. This is explained herein based on the section considered for the calculation of the bending resistance. The section used for the stress block method is located at mid-span (region of maximum bending moment) and there was no filling concrete in the PCHCS, as shown in **Fig. 24**. It was verified that for the studied models, there are only two possible positions for the P.N.A, depending on the geometric parameters, as well as the materials strength: P.N.A lies on flange or web. This implies that even if the filling concrete was considered, this resistance would be disregarded, since all the concrete below of P.N.A would be in tension.

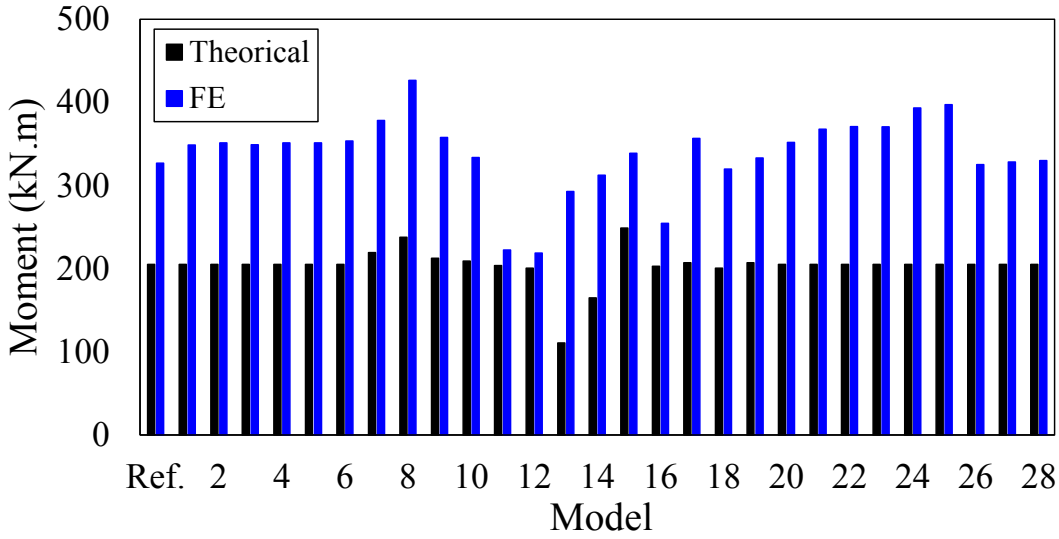

Fig. 25: Finite element vs. theorical

Concludings remarks

The present paper aimed to study the flexural behavior of steel-concrete composite cellular slim floor, considering the precast hollow-core slab. A finite element model was developed to predict the resistance of this structural system. The validation study was based on tests of steel-concrete composite slim floors. A parametric study was developed, varying the geometric and physical characteristics of the models. It was concluded:

i. The reference model, without the steel tie bar, had the lowest resistance and stiffness. The other models with crossbars showed higher values of resistance with slight variation in the values of applied force and vertical displacement, indicating limitations in the contribution of the steel tie bar. Models with greater diameter and quantity of steel tie bars showed greater resistance, but the contribution was insignificant. As a reference, the amount of two bars

with a diameter of 12.5 mm is indicated as the minimum limit for application in this type of composite section.

ii. Increasing the thickness of the concrete topping increased the resistance and stiffness of the composite section. The variation of the reinforcement ratio for cracking control showed a very slight influence on the resistance but indicated a relevant contribution in the cracking control.

iii. In Huo and D'Mello [37] was verified, considering pushout tests, that the shear connection resistance increased with increase of the web opening diameter and concrete strength. However, in the present work, considering the flexural behavior, the results indicated that an increase in the diameter of the openings, and the consequent increase of the area of the concrete dowel, does not increase the resistance of the USFBs. The model with an opening of 160 mm showed a reduction of more than 32% of the applied force in relation to the reference model.

iv. The stress and damage analyses provided evidence that the first failure mode of the reference model was the concrete crushing, followed by yielding of the cellular beam in the region of the supports.

v. The reduction in the thickness of the lower flange indicated a drop in resistance and a loss of stiffness. The variation in the thickness of the upper flange did not present a considerable influence, due to the strong contribution of the concrete slab to the compressive strength.

vi. The theoretical model underestimated the resistance of ultra-shallow floor beams with precast hollow-core slab. In this context, further

investigations are necessary, mainly for the study of concrete encasement and its contribution on bearing capacity.

References

[1] Hicks S. Current trend in modern floor construction. Mag Br Constr Steelwork Assoc (BCSA) 2003;11:32–3.

[2] Ju YK, Kim J-Y, Kim S-D. Experimental Evaluation of New Concrete Encased Steel Composite Beam to Steel Column Joint. Journal of Structural Engineering 2007;133:519–29. https://doi.org/10.1061/(ASCE)0733-9445(2007)133:4(519).

[3] Ahmed IM, Tsavdaridis KD. The evolution of composite flooring systems: applications, testing, modelling and eurocode design approaches. J Constr Steel Res 2019;155:286–300. https://doi.org/10.1016/j.jcsr.2019.01.007.

[4] Derkowski W, Surma M. Prestressed hollow core slabs for topped slim floors – Theory and research of the shear capacity. Eng Struct 2021;241:112464. https://doi.org/10.1016/j.engstruct.2021.112464.

[5] Wallin L. Technical and Economic Advantages of Steel Construction, Building Costs and Overall Economy. ECCS Publication: European Convention for Constructional Stelwork 1978.

[6] Lu X, Mäkeläinen P. Slim Floor Developments in Sweden and Finland. Structural Engineering International 1996;6:127–9. https://doi.org/10.2749/101686696780495789.

[7] Mullett DL, Lawson RM. Slim floor construction using deep decking. SCI-P127. London: The Steel Construction Institute; 1993.

[8] Lawson RMM, Lim J, Hicks SJJ, Simms WII. Design of composite asymmetric cellular beams and beams with large web openings. J Constr Steel Res 2006;62:614–29. https://doi.org/10.1016/j.jcsr.2005.09.012.

[9] Lawson RM, Saverirajan AHA. Simplified elasto-plastic analysis of composite beams and cellular beams to Eurocode 4. J Constr Steel Res 2011;67:1426–34. https://doi.org/10.1016/j.jcsr.2011.03.016.

[10] Ferreira FPV, Martins CH, De Nardin S. Advances in composite beams with web openings and composite cellular beams. J Constr Steel Res 2020;172:106182. https://doi.org/10.1016/j.jcsr.2020.106182.

[11] Coldebella G, Ferreira FPV, De Nardin S. Shear forces transfer in steel-concrete slim floor with circular web opening and PCHCS. Structures 2022;38:1295–307. https://doi.org/10.1016/j.istruc.2022.02.066.

[12] Ferreira FPV, Martins CH, De Nardin S. A parametric study of steel-concrete composite beams with hollow core slabs and concrete topping. Structures 2020;28:276–96. https://doi.org/10.1016/j.istruc.2020.08.045.

[13] Ferreira FPV, Tsavdaridis KD, Martins CH, De Nardin S. Ultimate strength prediction of steel–concrete composite cellular beams with PCHCS. Eng Struct 2021;236:112082. https://doi.org/10.1016/j.engstruct.2021.112082.

[14] Ferreira FPV, Tsavdaridis KD, Martins CH, De Nardin S. Composite action on web-post buckling shear resistance of composite cellular

beams with PCHCS and PCHCSCT. Eng Struct 2021;246:113065. https://doi.org/10.1016/j.engstruct.2021.113065.

[15] Shamass R, Ferreira FPV, Limbachiya V, Santos LFP, Tsavdaridis KD. Web-post buckling prediction resistance of steel beams with elliptically-based web openings using artificial neural networks (ANN). Thin-Walled Structures 2022;180:109959. https://doi.org/10.1016/j.tws.2022.109959.

[16] Ferreira FPV, Shamass R, Santos LFP, Limbachiya V, Tsavdaridis KD. EC3 design of web-post buckling resistance for perforated steel beams with elliptically-based web openings. Thin-Walled Structures 2022;175:109196. https://doi.org/10.1016/j.tws.2022.109196.

[17] Dong Y, Jia L, Xu F, Li X. Experimental study on seismic behavior of steel structure with cellular beams and composite concrete slab. Structures 2021;34:507–22. https://doi.org/10.1016/j.istruc.2021.07.081.

[18] Tsavdaridis KD. Structural performance of perforated steel beams with novel web openings and with partial concrete encasement. Doctoral Thesis. City University London, 2010. https://openaccess.city.ac.uk/id/eprint/11660/

[19] Hosseinpour E, Baharom S, W. Badaruzzaman WH, Al Zand AW. Push-out test on the web opening shear connector for a slim-floor steel beam: Experimental and analytical study. Eng Struct 2018;163:137–52. https://doi.org/10.1016/j.engstruct.2018.02.047.

[20] Limazie T, Chen S. Effective shear connection for shallow cellular composite floor beams. J Constr Steel Res 2017;128:772–88. https://doi.org/10.1016/j.jcsr.2016.10.010.

[21] Chen S, Limazie T, Tan J. Flexural behavior of shallow cellular composite floor beams with innovative shear connections. J Constr Steel Res 2015;106:329–46. https://doi.org/10.1016/j.jcsr.2014.12.021.

[22] Sheehan T, Dai X, Lam D, Aggelopoulos E, Lawson M, Obiala R. Experimental study on long spanning composite cellular beam under flexure and shear. J Constr Steel Res 2016;116:40–54. https://doi.org/10.1016/j.jcsr.2015.08.047.

[23] Kloeckner metals. USFB® - ULTRA SHALLOW FLOOR BEAM n.d.

[24] Lam D. Composite steel beams with precast hollow core slabs: behaviour and design. Progress in Structural Engineering and Materials 2002;4:179–85. https://doi.org/10.1002/pse.128.

[25] De Nardin S, Debs A El. State of the art of steel–concrete composite structures in Brazil. Proceedings of the Institution of Civil Engineers - Civil Engineering 2013;166:20–7. https://doi.org/10.1680/cien.2013.166.6.20.

[26] Ibrahim IS, Elliott KS, Abdullah R, Kueh ABH, Sarbini NN. Experimental study on the shear behaviour of precast concrete hollow core slabs with concrete topping. Eng Struct 2016;125:80–90. https://doi.org/10.1016/j.engstruct.2016.06.005.

[27] Hicks SJ, Lawson RM. Design of composite beams using precast concrete slabs. SCI P287. The Steel Construction Institute; 2003.

663 [28] Lam D. Capacities of headed stud shear connectors in composite steel
664 beams with precast hollowcore slabs. J Constr Steel Res 2007;63:1160–
665 74. https://doi.org/10.1016/j.jcsr.2006.11.012.
666 [29] Pajari M, Koukkari H. Shear Resistance of PHC Slabs Supported on
667 Beams. I: Tests. Journal of Structural Engineering 1998;124:1062–73.
668 https://doi.org/10.1061/(ASCE)0733-9445(1998)124:9(1050).
669 [30] Pajari M. Shear Resistance of PHC Slabs Supported on Beams. II:
670 Analysis. Journal of Structural Engineering 1998;124:1062–73.
671 https://doi.org/10.1061/(ASCE)0733-9445(1998)124:9(1062).
672 [31] Hegger J, Roggendorf T, Kerkeni N. Shear capacity of prestressed
673 hollow core slabs in slim floor constructions. Eng Struct 2009;31:551–9.
674 https://doi.org/10.1016/j.engstruct.2008.10.006.
675 [32] Gouchman GH. Design of composite beams using precast concrete slabs
676 in accordance with EUROCODE 4. SCI P401. The Steel Construction
677 Institute; 2014.
678 [33] Baran E. Effects of cast-in-place concrete topping on flexural response
679 of precast concrete hollow-core slabs. Eng Struct 2015;98:109–17.
680 https://doi.org/10.1016/j.engstruct.2015.04.017.
681 [34] Girhammar UA, Pajari M. Tests and analysis on shear strength of
682 composite slabs of hollow core units and concrete topping. Constr Build
683 Mater 2008;22:1708–22.
684 https://doi.org/10.1016/j.conbuildmat.2007.05.013.

[35] Huo BY. Experimental and analytical study of the shear transfer in composite shallow cellular floor beams. Doctoral Thesis. City University London, 2012. https://openaccess.city.ac.uk/id/eprint/1965/

[36] Tsavdaridis KD, D'Mello C, Hawes M. Experimental study of ultra shallow floor beams (USFB) with perforated steel sections. The 11th Nordic Steel Construction Conference 2009 (NSCC 2009), Malmö, Sweden: 2009, p. 312–9.

[37] Huo BY, D'Mello CA. Push-out tests and analytical study of shear transfer mechanisms in composite shallow cellular floor beams. J Constr Steel Res 2013;88:191–205. https://doi.org/10.1016/j.jcsr.2013.05.007.

[38] Huo BY, D'Mello CA. Shear Transferring Mechanisms in a Composite Shallow Cellular Floor Beam with Web Openings. Structures 2017;9:134–46. https://doi.org/10.1016/j.istruc.2016.11.003.

[39] Braun M, Obiala R, Odenbreit C. Analyses of the loadbearing behaviour of deep-embedded concrete dowels, CoSFB. Steel Construction 2015;8:167–73. https://doi.org/10.1002/stco.201510024.

[40] Limazie T, Chen S. FE modeling and numerical investigation of shallow cellular composite floor beams. J Constr Steel Res 2016;119:190–201. https://doi.org/10.1016/j.jcsr.2015.12.022.

[41] Ryu J, Lee C-H, Oh J, Yoon S-W, Ju YK. Shear Resistance of a Biaxial Hollow Composite Floor System with GFRP Plates. Journal of Structural Engineering 2017;143:04016180. https://doi.org/10.1061/(ASCE)ST.1943-541X.0001657.

[42] Dai X, Lam D, Sheehan T, Yang J, Zhou K. Effect of dowel shear connector on performance of slim-floor composite shear beams. J Constr Steel Res 2020;173:106243. https://doi.org/10.1016/j.jcsr.2020.106243.

[43] de O. Ferrante CA, de Andrade SAL, de Lima LRO, da S. Vellasco PCG. Analytical study and experimental tests on innovative steel-concrete composite floorings. J Constr Steel Res 2020;168:105868. https://doi.org/10.1016/j.jcsr.2019.105868.

[44] Alam N, Nadjai A, Hanus F, Kahanji C, Vassart O. Experimental and numerical investigations on slim floor beams exposed to fire. Journal of Building Engineering 2021;42:102810. https://doi.org/10.1016/j.jobe.2021.102810.

[45] Kyriakopoulos P, Peltonen S, Vayas I, Spyrakos C, Leskela M v. Experimental and numerical investigation of the flexural behavior of shallow floor composite beams. Eng Struct 2021;231:111734. https://doi.org/10.1016/j.engstruct.2020.111734.

[46] Dassault Systèmes Simulia. Abaqus 6.18 2016.

[47] Souza PT de. Análise teórica e experimental de pisos mistos de pequena altura compostos por vigas metálicas e lajes alveolares de concreto. Universidade de São Paulo, 2016. https://doi.org/10.11606/D.18.2016.tde-06042016-112204.

[48] Hillerborg A, Modéer M, Petersson P-E. Analysis of crack formation and crack growth in concrete by means of fracture mechanics and finite elements. Cem Concr Res 1976;6:773–81. https://doi.org/10.1016/0008-8846(76)90007-7.

[49] Lubliner J, Oliver J, Oller S, Oñate E. A plastic-damage model for concrete. Int J Solids Struct 1989;25:299–326. https://doi.org/10.1016/0020-7683(89)90050-4.

[50] Lee J, Fenves GL. Plastic-Damage Model for Cyclic Loading of Concrete Structures. J Eng Mech 1998;124:892–900. https://doi.org/10.1061/(ASCE)0733-9399(1998)124:8(892).

[51] Rewers I. Numerical Analysis of RC beam with High Strength Steel Reinforcement using CDP model. IOP Conf Ser Mater Sci Eng 2019;471:022025. https://doi.org/10.1088/1757-899X/471/2/022025.

[52] Behnam H, Kuang JS, Samali B. Parametric finite element analysis of RC wide beam-column connections. Comput Struct 2018;205:28–44. https://doi.org/10.1016/j.compstruc.2018.04.004.

[53] Nguyen TNH, Tan KH, Kanda T. Investigations on web-shear behavior of deep precast, prestressed concrete hollow core slabs. Eng Struct 2019;183:579–93. https://doi.org/10.1016/j.engstruct.2018.12.052.

[54] Qureshi J, Lam D, Ye J. Finite element modelling of shear connection behaviour in a push test using profiled sheeting. Advances and Trends in Structural Engineering, Mechanics and Computation - Proceedings of the 4th International Conference on Structural Engineering, Mechanics and Computation, SEMC 2010 2010:679–82.

[55] Genikomsou AS, Polak MA. Finite element analysis of punching shear of concrete slabs using damaged plasticity model in ABAQUS. Eng Struct 2015;98:38–48. https://doi.org/10.1016/j.engstruct.2015.04.016.

[56] Earij A, Alfano G, Cashell K, Zhou X. Nonlinear three–dimensional finite–element modelling of reinforced–concrete beams: Computational challenges and experimental validation. Eng Fail Anal 2017;82:92–115. https://doi.org/10.1016/j.engfailanal.2017.08.025.

[57] Katwal U, Tao Z, Uy B, Hassan MK, Uy B, Lam D. Load sharing mechanism between shear studs and profiled steel sheeting in push tests. J Constr Steel Res 2020;174:106279. https://doi.org/10.1016/j.jcsr.2020.106279.

[58] European committee for standardization. Eurocode 2: Design of concrete structures - Part 1-1 : General rules and rules for buildings 2004.

[59] Xu C, Sugiura K, Wu C, Su Q. Parametrical static analysis on group studs with typical push-out tests. J Constr Steel Res 2012;72:84–96. https://doi.org/10.1016/j.jcsr.2011.10.029.

[60] Pavlović M, Marković Z, Veljković M, Buđevac D. Bolted shear connectors vs. headed studs behaviour in push-out tests. J Constr Steel Res 2013;88:134–49. https://doi.org/10.1016/j.jcsr.2013.05.003.

[61] Ministry of Construction of the People's Republic of China. NATIONAL STANDARD OF THE PEOPLE'S REPUBLIC OF CHINA. GB 50010-2002: Code for Design Concrete Structures 2002:1–357.

[62] Byfield MP, Davies JM, Dhanalakshmi M. Calculation of the strain hardening behaviour of steel structures based on mill tests. J Constr Steel Res 2005;61:133–50. https://doi.org/10.1016/j.jcsr.2004.08.001.

779 [63] Tsavdaridis KD, D'Mello C, Huo BY. Experimental and computational
780 study of the vertical shear behaviour of partially encased perforated
781 steel beams. Eng Struct 2013;56:805–22.
782 https://doi.org/10.1016/j.engstruct.2013.04.025.
783 [64] Tsavdaridis KD, D'Mello C, Huo BY. Computational Study Modelling
784 the Experimental Work Conducted on the Shear Capacity of Perforated
785 Concrete-Steel Ultra Shallow Floor Beams (USFB). The 16th National
786 Concrete Conference, Paphos, Cyprus: n.d.
787 https://doi.org/https://doi.org/10.31224/2149.
788 [65] Guezouli S, Lachal A. Numerical analysis of frictional contact effects in
789 push-out tests. Eng Struct 2012;40:39–50.
790 https://doi.org/10.1016/j.engstruct.2012.02.025.
791 [66] Araújo D de L. Cisalhamento na interface entre concreto pré-moldado e
792 concreto moldado no local em elementos submetidos à flexão.
793 Universidade de São Paulo, 1997.
794 [67] 318 AC. Building code requirements for structural concrete : (ACI 318-
795 14). Farmington Hills, MI : American Concrete Institute, [1995] ©1995;
796 n.d.
797 [68] Katwal U, Tao Z, Hassan MK. Finite element modelling of steel-
798 concrete composite beams with profiled steel sheeting. J Constr Steel
799 Res 2018;146:1–15. https://doi.org/10.1016/j.jcsr.2018.03.011.
800 [69] Lawson RM, Hicks SJ. Design of composite beams with large web
801 openings. SCI P355. The Steel Construction Institute; 2011.
802